Forward-scattering magneto-optical effects

Isao Hirano
National Research Laboratory of Metrology, 1-4 Umezono 1-chome, Tsukuba, Ibaraki 305, Japan
(Received 2 March 1995; revised manuscript received 7 July 1995)

A general equation is constructed for magneto-optical spectra. The incident laser beam has an arbitrary polarization and its direction is arbitrary relative to the magnetic field. The analyzer has an arbitrary extinction ratio function. The Faraday and Voigt formulas are deduced as special solutions. From the generalized Faraday formula, the absorption spectra of σ^+ and σ^- light are measured without influence of the birefringence. The circular dichroism is estimated. The measured spectra clearly show the frequency shifts of σ^+ and σ^- light. The magnitude of the shift for a magnetic field of 0.015 T is twice as large as the Doppler width for the Cs D_2 line. These shifts are induced by the Larmor precession defined by the fine-structure g factor. The Larmor precession does not induce a real shift of Zeeman levels, but induces a phase shift of optical coherence through the Rabi frequency.

PACS number(s): 32.60.+i, 32.70.Jz, 32.30.−r

I. INTRODUCTION

Forward-scattering magneto-optical effects such as the Faraday and Voigt effects have been studied extensively by a large number of authors (see [1–9] and references therein). In particular, the Cs D_2 line has been studied mainly on the Faraday rotation angle by Chen, Telegdi, and Weiss [10] and Kanorsky *et al.* [11]. The spectral profiles and relevant theory still need to be investigated further. All studies to date have been based on the fundamental and specific formulas of Faraday and Voigt. The application of these formulas is limited to the special case where the incident light is linearly polarized and the exctinction ratio function of the analyzer is also linear.

In the Faraday formula, the incident light must be parallel to the magnetic field. Moreover, the Faraday rotation angle (birefringence) and absorption terms (circular dichroism) are closely related to each other and cannot be separated. In the Voigt formula, the light must be incident perpendicular to the field and the polarization plane of the incident light must be perpendicular (σ eigenwave) or parallel (π eigenwave) to the direction of the static homogeneous magnetic field.

In our previous paper [12], we analyzed the case where light is incident at an arbitrary direction to the magnetic field, from which the Faraday and Voigt formulas have been derived as special solutions. In our present approach to magneto-optical spectra, we have expanded the theory of linear polarizers to the more general case. This general equation also makes it possible to derive Faraday and Voigt spectra as special solutions. The spectral profiles can be investigated for arbitrary polarization of the incident laser beam such as linear, elliptical, or circular polarizations. In addition, the analyzer can possess an arbitrary extinction ratio function that is linear, elliptical, or rectangular. The direction of propagation of laser beam is arbitrary with respect to the magnetic field.

By taking advantage of one of the special solutions of the generalized Faraday formula, the absorption profiles of σ^+ and σ^- light can be measured independently without the influence of the Faraday rotation. Therefore, the circular dichroism (magnetic-field-induced optical rotation) can be evaluated.

In our experiment of Faraday geometry, a clear frequency shift is observed between σ^+ and σ^- polarized light. All σ^+ lines shift together in the same direction and all σ^- lines in the reverse direction. The magnitude of the shift for a magnetic field of 0.015 T is twice as large as the Doppler width for the Cs D_2 line. This shift originates in the Larmor precession of the Cs atom and does not depend on the real level splittings. The level splittings are not always linear with the magnetic field: the classical vector model is not always valid.

II. THEORY

A. Light electric field

Figure 1 shows the geometry for the observation of forward-scattered magneto-optical spectra. The axis $\vec{e}_{\varepsilon_1}$ defines the electric field of the light (see captions)

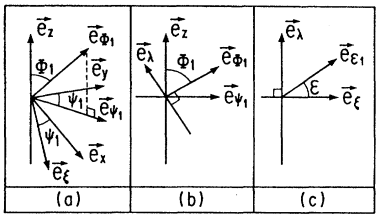

FIG. 1. Applied homogeneous magnetic field in the $\vec{e}_z$ direction. (a) Axes $\vec{e}_x$, $\vec{e}_y$, and $\vec{e}_z$ constitute an orthogonal set of Cartesian coordinates. The axis $\vec{e}_{\phi_1}$ shows the direction of propagation of the laser beam and is contained in the $(\vec{e}_{\psi_1}, \vec{e}_z)$ plane. Axes $\vec{e}_\xi, \vec{e}_{\psi_1}$ correspond to axes $\vec{e}_x, \vec{e}_y$ rotated by an angle ψ_1 around the $\vec{e}_z$ axis. (b) $\vec{e}_\xi$ perpendicular to the page. The plane spanned by the axes $\vec{e}_\lambda$ and $\vec{e}_\xi$ is perpendicular to the direction of laser beam $(\vec{e}_{\Phi_1})$. The electric field of light is in the plane $(\vec{e}_\xi, \vec{e}_\lambda)$. (c) Axis $\vec{e}_{\varepsilon_1}$ defines the electric field of the light.

$$\vec{e}_{\varepsilon_1}=\begin{bmatrix}E_1^x\\E_1^y\\E_1^z\end{bmatrix}=\begin{bmatrix}\cos\psi_1\cos\varepsilon-\sin\psi_1\cos\Phi_1\sin\varepsilon\\-\sin\psi_1\cos\varepsilon-\cos\psi_1\cos\Phi_1\sin\varepsilon\\\sin\Phi_1\sin\varepsilon\end{bmatrix}. \quad (1)$$

The direction perpendicular to $\vec{e}_{\varepsilon_1}$ is expressed by $\vec{e}_{\varepsilon_2}$

$$\vec{e}_{\varepsilon_2}=\begin{bmatrix}E_2^x\\E_2^y\\E_2^z\end{bmatrix}=\begin{bmatrix}-\cos\psi_1\sin\varepsilon-\sin\psi_1\cos\Phi_1\cos\varepsilon\\\sin\psi_1\sin\varepsilon-\cos\psi_1\cos\Phi_1\cos\varepsilon\\\sin\Phi_1\cos\varepsilon\end{bmatrix}. \quad (2)$$

Therefore, the incident elliptically polarized laser beam may be expressed as

$$\vec{E}(0,t)=E_0a_1\cos\omega t\begin{bmatrix}E_1^x\\E_1^y\\E_1^z\end{bmatrix}+E_0a_2\sin\omega t\begin{bmatrix}E_2^x\\E_2^y\\E_2^z\end{bmatrix}, \quad (3)$$

where a_1 and a_2 are the major and minor axes of the ellipse, respectively. When the electric field of the light rotates in the opposite sense, the coefficient a_2 becomes $-a_2$.

Here we seek a propagating electric field of light in the form

$$\vec{E}(z,t)=(E_0/2)[A_+\vec{e}_+e^{-i(\omega t-k_+z)}+A_-\vec{e}_-e^{-i(\omega t-k_-z)}+A_\pi\vec{e}_\pi e^{-i(\omega t-k_\pi z)}+\text{c.c.}], \quad (4)$$

where $A_{\pm,\pi}$ is a proportional constant and $k_{\pm,\pi}$ is the complex wave number for the $\sigma^{\pm}$ and π components, respectively. The vectors $\vec{e}_\pm$ and $\vec{e}_\pi$ constitute a spherical coordinate system, i.e., $\vec{e}_\pm=\mp(1/\sqrt{2})(\vec{e}_x\pm i\vec{e}_y)$, $\vec{e}_\pi=\vec{e}_z$.

From the boundary conditions for Eqs. (3) and (4), the electric field transmitted through the absorption cell is obtained in the form

$$\vec{E}(s,t)=[E_{xt},E_{yt},E_{zt}], \quad (5a)$$

where

$$E_{xt}=(E_0/2)[e^{-k_+^i s},e^{-k_-^i s}]\left\{a_1\begin{bmatrix}E_1^x\cos R_+-E_1^y\sin R_+\\E_1^x\cos R_-+E_1^y\sin R_-\end{bmatrix}+a_2\begin{bmatrix}E_2^y\cos R_++E_2^x\sin R_+\\-E_2^y\cos R_-+E_2^x\sin R_-\end{bmatrix}\right\}, \quad (5b)$$

$$E_{yt}=(E_0/2)[e^{-k_+^i s},e^{-k_-^i s}]\left\{a_1\begin{bmatrix}E_1^y\cos R_++E_1^x\sin R_+\\E_1^y\cos R_--E_1^x\sin R_-\end{bmatrix}+a_2\begin{bmatrix}-E_2^x\cos R_++E_2^y\sin R_+\\E_2^x\cos R_-+E_2^y\sin R_-\end{bmatrix}\right\}. \quad (5c)$$

$$E_{zt}=E_0[e^{-k_\pi^i s}]\{a_1[E_1^z\cos R_\pi]+a_2[E_2^z\sin R_\pi]\}. \quad (5d)$$

The symbols $R_\pm$ and R_π are defined as $\omega t-k_\pm^r s$ and $\omega t-k_\pi^r s$, respectively. s refers to the length of the cell and $E_1^x,\ldots,E_2^x,\ldots$ are as defined in Eqs. (1) and (2).

B. Observed spectra

The plane of polarization of the analyzer is expressed analogously to Eq. (1) by (see Fig. 1 and its caption)

$$\vec{e}_{\theta_1}=\begin{bmatrix}S_1^x\\S_1^y\\S_1^z\end{bmatrix}=\begin{bmatrix}\cos\psi_2\cos\theta-\sin\psi_2\cos\Phi_2\sin\theta\\-\sin\psi_2\cos\theta-\cos\psi_2\cos\Phi_2\sin\theta\\\sin\Phi_2\sin\theta\end{bmatrix}. \quad (6)$$

The axis perpendicular to $\vec{e}_{\theta_1}$ is described by $\vec{e}_{\theta_2}$,

$$\vec{e}_{\theta_2}=\begin{bmatrix}S_2^x\\S_2^y\\S_2^z\end{bmatrix}=\begin{bmatrix}-\cos\psi_2\sin\theta-\sin\psi_2\cos\Phi_2\cos\theta\\\sin\psi_2\sin\theta-\cos\psi_2\cos\Phi_2\cos\theta\\\sin\Phi_2\cos\theta\end{bmatrix}. \quad (7)$$

When the extinction ratio function of the analyzer is elliptical, it may be written as

$$\vec{E}_\delta=b_1\cos\delta\begin{bmatrix}S_1^x\\S_1^y\\S_1^z\end{bmatrix}+b_2\sin\delta\begin{bmatrix}S_2^x\\S_2^y\\S_2^z\end{bmatrix}, \quad (8)$$

where b_1 and b_2 are the major and minor axes, respectively. The symbol δ refers to the angle measured from the axis $\vec{e}_{\theta_1}$. The light transmitted through the analyzer is given by the square of the inner product of the vector of the electric field of the light and that of the analyzer and by integrating over the exctinction ratio function. Therefore, we obtain the spectral profiles observed through the analyzer as follows:

$$\begin{aligned}I_\theta\propto\int_0^{2\pi}[\vec{E}(s,t)\cdot\vec{E}_\delta]^2d\delta&=\int_0^{2\pi}\left\{[E_{xt},E_{yt},E_{zt}]\left(b_1\cos\delta\begin{bmatrix}S_1^x\\S_1^y\\S_1^z\end{bmatrix}+b_2\sin\delta\begin{bmatrix}S_2^x\\S_2^y\\S_2^z\end{bmatrix}\right)\right\}^2d\delta\\&=[(b_1)^2/2][(S_1^x)^2(E_{xt})^2+(S_1^y)^2(E_{yt})^2+(S_1^z)^2(E_{zt})^2\\&\quad+2S_1^xS_1^y(E_{xt}E_{yt})+2S_1^yS_1^z(E_{yt}E_{zt})+2S_1^xS_1^z(E_{zt}E_{xt})]\\&\quad+[(b_2)^2/2][(S_2^x)^2(E_{xt})^2+(S_2^y)^2(E_{yt})^2\\&\quad+(S_2^z)^2(E_{zt})^2+2S_2^xS_2^y(E_{xt}E_{yt})+2S_2^yS_2^z(E_{yt}E_{zt})+2S_2^xS_2^z(E_{zt}E_{xt})],\end{aligned} \quad (9)$$

where the rotating-wave approximation (rapidly oscillating terms are neglected) is assumed and the extinction ratio function $\vec{E}_\delta$ may assume an arbitrary form: rectangular or any closed curve.

C. Generalized Faraday formula

The Faraday formula is deduced as a special solution of this general equation. When the light propagates along the magnetic-field direction and the plane of the analyzer is perpendicular to the laser beam $\Phi_1=0, \Phi_1=\Phi_2$ and $\psi_1=\psi_2$. Therefore the Faraday spectrum for an elliptically polarized incident laser beam and an elliptical extinction ratio function of the analyzer is obtained as follows:

$$I_\theta \propto (E_0^2/16)\{(b_1^2+b_2^2)(e^{-2k_+^i s}(a_1-a_2)^2+e^{-2k_-^i s}(a_1+a_2)^2 + 2(a_1^2-a_2^2)(b_1^2-b_2^2)e^{-k_+^i s}e^{-k_-^i s}\cos[2(\varepsilon-\theta) + (k_+^r-k_-^r)s]\}. \quad (10)$$

For circularly polarized incident light ($a_1=a_2$), the Faraday spectra give an absorption profile of either right or left circularly polarized light and the interference term vanishes. When the analyzer is absent ($b_1=b_2$), the Faraday spectra possess only absorption profiles. These facts may be combined to extract the circular dichroism ($[k_+^i-k_-^i]s/2$, for small $k_\pm^i$, the parity nonconserving rotation [10,13]) without the influence of birefringence ($[k_+^r-k_-^r]s/2$, the Faraday rotation).

For linearly polarized light ($a_1=1$, $a_2=0$) and a linear extinction ratio function of the analyzer ($b_1=1$, $b_2=0$), the ordinary Faraday formula is obtained.

For the case where the analyzer is not perpendicular to the light beam, the spectra are different from those for the perpendicular case. For example, the Faraday spectra for $\psi_1=\psi_2=0$, $\Phi_1=0$, and $\Phi_2\neq 0$ are given by

$$I_\theta \propto (E_0^2/16)(B_+[(a_1-a_2)^2e^{-2k_+^i s}+(a_1+a_2)^2e^{-2k_-^i s}] + B_0\{(B_-)\cos[2\varepsilon+(k_+^r-k_-^r)s]+(b_1^2-b_2^2) \times \cos\Phi_2 \sin 2\theta \sin[2\varepsilon+(k_+^r-k_-^r)s]\}), \quad (11a)$$

where

$$B_\pm = b_1^2(\cos^2\theta \pm \cos^2\Phi_2\sin^2\theta)+b_2^2(\sin^2\theta\pm\cos^2\Phi_2\cos^2\theta) \quad (11b)$$

and

$$B_0 = 2(a_1^2-a_2^2)e^{-k_+^i s}e^{-k_-^i s}. \quad (11c)$$

When $\Phi_2=0$, Eq. (11a) reduces to Eq. (10).

D. Generalized Voigt formula

For the Voigt spectra $\Phi_1=\pi/2$, $\Phi_2=\Phi_1$, and $\psi_1=\psi_2$. Therefore, the σ component is obtained when $\varepsilon=0$:

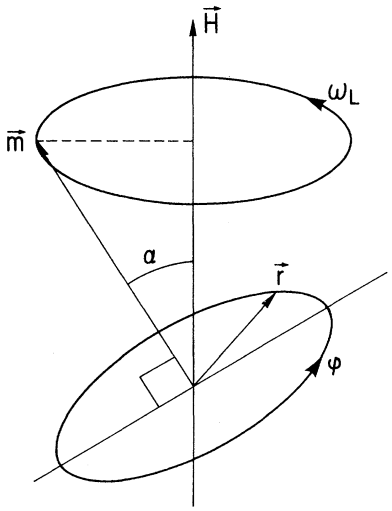

FIG. 2. Larmor precession of a magnetic dipole moment $\vec{m}$ and a relevant valence electron orbit with angular frequency φ. $\vec{H}$ shows the magnetic field. The electric dipole moment is $\vec{\mu}=-e\vec{r}$.

$$I_\theta \propto (E_0^2/16)[a_1^2(b_1^2\cos^2\theta+b_2^2\sin^2\theta)\{e^{-2k_+^i s}+e^{-2k_-^i s} + 2e^{-k_+^i s}e^{-k_-^i s}\cos(R_+-R_-)\}-2a_1a_2 \times (b_1^2-b_2^2)\sin(2\theta)e^{-k_\pi^i s}\{e^{-k_+^i s}\sin(R_+-R_\pi)-e^{-k_-^i s} \times \sin(R_--R_\pi)\}+4a_2^2(b_1^2\sin^2\theta+b_2^2\cos^2\theta)e^{-2k_\pi^i s}]. \quad (12)$$

When the analyzer is absent ($b_1=b_2$) the Voigt spectra have an interference term between right and left circularly polarized light as well as absorption terms. For $a_1=1$, $a_2=0$, $b_1=1$, and $b_2=0$, the Voigt spectrum for a σ-polarized eigenwave with a linearly polarized laser beam and a linear analyzer extinction ratio function is obtained:

$$I_\theta \propto \cos^2(\theta)\{(1/2)(e^{-2k_+^i s}+e^{-2k_-^i s}) + \cos[(k_+^r-k_-^r)s]e^{-(k_+^i+k_-^i)s}\}. \quad (13)$$

The σ component has an interference term as well as absorption terms.

For π-polarized light of Voigt geometry $\varepsilon=\pi/2$. In this case, the spectrum is obtained by interchanging a_1 and a_2 in Eq. (12). For linearly polarized light ($a_1=1$, $a_2=0$) and a linear analyzer extinction ratio function ($b_1=1$, $b_2=0$), the absorption spectrum of the eigenwave π is obtained:

$$I_\theta \propto 2\ \sin^2(\theta)e^{-2k_\pi^i s}. \quad (14)$$

The π component spectra have simple absorption profiles. For Voigt spectra [Eqs. (13) and (14)], the profiles of eigenwaves σ and π are not influenced by the angle (θ) of polarization of the analyzer; only their intensity is modified.

E. Complex wave-number

Figure 2 shows the precession of the magnetic dipole moment $\vec{m}$ around a magnetic field $\vec{H}$ with Larmor frequency

ω_L. The electric dipole moment $\vec{\mu}$ precesses in the plane perpendicular to the magnetic moment with an angular frequency φ. When the Larmor frequency is small compared to the angular frequency of the valence electron, the electric-dipole moment can be written as [12,14]

$$\vec{\mu}=\begin{bmatrix}\mu_x\\ \mu_y\\ \mu_z\end{bmatrix}\approx(\mu/\sqrt{2})\begin{bmatrix}\cos\alpha\ \cos\omega_L t+\sin\omega_L t\\ \cos\alpha\ \sin\omega_L t-\cos\omega_L t\\ -\sin\alpha\end{bmatrix}. \quad (15)$$

For a cesium atom, $\varphi\approx 10^{14}$ Hz and $\omega_L\approx 10^8$ Hz at 0.015 T.

In the first stage of density-matrix formalism, the wave number k is usually regarded as real. Therefore, from Eqs. (4) and (15), the Rabi frequency is deduced as follows [12]:

$$\begin{aligned}\vec{E}(z,t)\cdot\vec{\mu}/\hbar=&(\mu E_0/4\sqrt{2}\hbar)\{e^{i(S_+-\omega_L t)}(f_+)[-\cos\alpha-i]\\&+e^{i(S_-+\omega_L t)}(f_-)(\cos\alpha-i)-2e^{iS_\pi}(f_\pi)(\sin\alpha)\\&+\text{c.c.}\},\end{aligned} \quad (16)$$

where $S_{\pm,\pi}=\omega t-k_{\pm,\pi}z$, $f_\pm=|f_\pm|e^{-i\eta_\pm}$, $f_\pi=|f_\pi|e^{-i\eta_\pi}$, and $-\eta_{\pm,\pi}$ is the angle between $|f_{\pm,\pi}|$ and $f^r_{\pm,\pi}$. The explicit expressions for $f_\pm$ and f_π are given by

$$f_+=f^r_+ + if^i_+=[a_1,a_2]\left\{\begin{bmatrix}-E_1^x\\ -E_2^y\end{bmatrix}+i\begin{bmatrix}-E_1^y\\ E_2^x\end{bmatrix}\right\}. \quad (17a)$$

$$f_-=f^r_- + if^i_-=[a_1,a_2]\left\{\begin{bmatrix}E_1^x\\ -E_2^y\end{bmatrix}+i\begin{bmatrix}-E_1^y\\ -E_2^x\end{bmatrix}\right\}. \quad (17b)$$

$$f_\pi=f^r_\pi+if^i_\pi=[a_1,a_2]\begin{bmatrix}E_1^z\\ -iE_2^z\end{bmatrix}, \quad (17c)$$

where $E_1^{x,y,z}, E_2^{x,y,z}$ are defined by Eqs. (1) and (2).

As the Rabi frequency is a proportional coefficient of optical coherence in the density-matrix formalism, which is defined by the Hamiltonian $H=H_0-\vec{\mu}\cdot\vec{E}$, in order to obtain the time-independent part of the density matrix by the rotating-wave approximation and to preserve the effectiveness of the usual framework of density matrix formalism, the following definition is necessary in view of Eq. (16):

$$\rho_\pm=\tilde{\rho}_\pm e^{i[(\omega\mp\omega_L)t-k_\pm z]}, \quad (18a)$$

$$\rho^t_\pm=\rho_\pm e^{i\eta_\pm}, \quad (18b)$$

where the optical coherence of σ^+ and σ^- light is shifted in phase in opposite directions by the Larmor precession. In analogy to Eq. (18), the optical coherence for π-polarized light has the form

$$\rho_\pi=\tilde{\rho}_\pi e^{i(\omega t-k_\pi z)}, \quad (19a)$$

$$\rho^t_\pi=\rho_\pi e^{i\eta_\pi}. \quad (19b)$$

The density-matrix equations defined by the Liouville equation are solved here for the two-level open system where the populations are not necessarily conserved for the relevant two levels, but an equilibrium is maintained by optical pumping and relaxation cycles (Fig. 3).

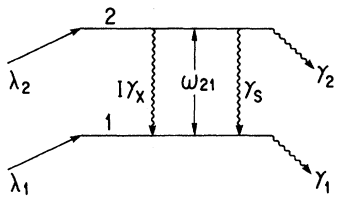

FIG. 3. Two-level open system. γ_1 refers to the ground-state relaxation rate, γ_2 to the excited-state relaxation rate, γ_s to the natural transition rate, and $I\gamma_x$ to the induced emission rate (I is a factor proportional to the laser intensity).

The macroscopic polarization of the medium and the susceptibility are obtained through this solution as [12,14]

$$\begin{aligned}P_{\pm,\pi}(z,t)=&N_0\int_{-\infty}^{\infty}[\mu^*_{\pm,\pi}\rho^t_{\pm,\pi}+\text{c.c}]d(kv)\\=&\tfrac{1}{2}\{\varepsilon_0E_0\chi_{\pm,\pi}e^{i(\omega t-k_{\pm,\pi}z)}+\text{c.c.}\},\end{aligned} \quad (20)$$

where the electric-dipole moment in the spherical coordinate system is given by $\mu_\pm=\mp(\mu/2)(\cos\alpha\pm i)e^{\mp i\omega_L t}$ and $\mu_\pi=-(\mu/\sqrt{2})\sin\alpha$. N_0 is the atomic density and $\chi_{\pm,\pi}=\chi^r_{\pm,\pi}-i\chi^i_{\pm,\pi}$. The susceptibility is derived for $\sigma^\pm$ light as [12,14]

$$\begin{aligned}\chi^r_\pm=&-C_\pm\int_{-\infty}^{\infty}\frac{(\omega\mp\omega_L-\omega_{21}-kv)}{(\omega\mp\omega_L-\omega_{21}-kv)^2+\gamma^2+2\gamma\delta|\beta_\pm|^2}\\&\times\exp[-(kv/\Delta\nu_D)^2]k\,dv,\end{aligned} \quad (21a)$$

$$\begin{aligned}\chi^i_\pm=&+C_\pm\int_{-\infty}^{\infty}\frac{\gamma}{(\omega\mp\omega_L-\omega_{21}-kv)^2+\gamma^2+2\gamma\delta|\beta_\pm|^2}\\&\times\exp[-(kv/\Delta\nu_D)^2]k\,dv,\end{aligned} \quad (21b)$$

where

$$C_\pm=|f_\pm|(1+\cos^2\alpha)(N_0/\varepsilon_0)[(\mu^\pm_{12})^2/\hbar]/[4\sqrt{2\pi}\Delta\nu_D], \quad (22)$$

$\gamma=(\gamma_1+\gamma_2+\gamma_s+I\gamma_x)/2$, and $\delta=(\gamma_1+\gamma_2)/[\gamma_1(\gamma_2+\gamma_s+I\gamma_x)]$. The electric-dipole moment μ and the transition probability B have the relation $\mu^2=3\varepsilon_0\hbar\lambda^3B/8\pi^2$.

The stationary Rabi frequency related to $\rho_{\pm,\pi}$ may be written as $\beta_\pm=|f_\pm|\mu_{12}E_0(-i\mp\cos\alpha)/4\sqrt{2}\hbar$ and $\beta_\pi=|f_\pi|\mu_{12}E_0(-\sin\alpha)/2\sqrt{2}\hbar$. As the transition probability is broadened by the laser spectral width ($\omega_{\rm LS}$) [15], the Rabi frequency β may be expressed as

$$|\beta_{\pm,\pi}|^2\Rightarrow\frac{|\beta_{\pm,\pi}|^2(\omega_{\rm LS})^2}{(\omega-\omega^{\pm,\pi}_{12}-kv)^2+(\omega_{\rm LS})^2}. \quad (23)$$

For π-polarized light, susceptibilities are obtained by assuming $\omega_L=0$ in Eq. (21) and the proportional coefficient is

$$C_\pi=|f_\pi|(\sin^2\alpha)(N_0/\varepsilon_0)[(\mu^\pi_{12})^2/\hbar]/[2\sqrt{\pi}\Delta\nu_D]. \quad (24)$$

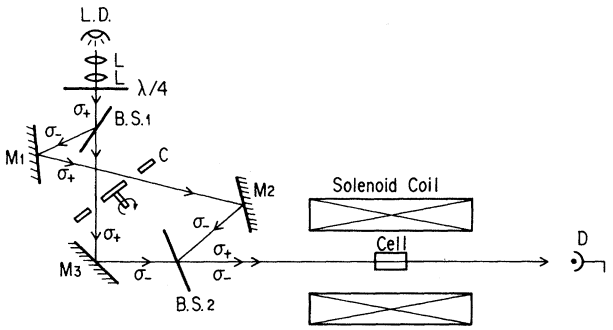

FIG. 4. Experimental block diagram. LD, laser diode; L, collimating lens; λ/4, quarter-wave plate; BS 1 and BS 2, beam splitters; M1, M2, and M3, mirrors; C, chopper; Cell, Cs absorption cell; D, detector. The applied magnetic field is 0.015 T.

The relations between the susceptibility and complex wave number are written as [12,14]

$$k^i_{\pm,\pi}=\frac{\sqrt{2}\pi}{\lambda}\{[(1+\chi^r_{\pm,\pi})^2+(\chi^i_{\pm,\pi})^2]^{1/2}-(1+\chi^r_{\pm,\pi})\}^{1/2}, \tag{25a}$$

$$k^r_{\pm,\pi}=\frac{\sqrt{2}\pi}{\lambda}\{[(1+\chi^r_{\pm,\pi})^2+(\chi^i_{\pm,\pi})^2]^{1/2}+(1+\chi^r_{\pm,\pi})\}^{1/2}. \tag{25b}$$

The magneto-optical spectra I_θ is deduced from these wave numbers.

III. EXPERIMENT

In order to observe both right and left circularly polarized light simultaneously, the instrumental arrangement shown in Fig. 4 is used. Right circularly polarized light reflected by a mirror is converted to left circularly polarized light and vice versa.

The method is based on Eq. (10). The analyzer is absent ($b_1=b_2$) and the incident light is circularly polarized ($a_1=a_2$). The chopper interrupts σ^+ and σ^- light reciprocally with a chopping frequency of around several hertz. When σ^+ light passes through the absorption cell, σ^- light does not exist in the cell and vice versa. Accordingly, the σ^+ and σ^- light are absorbed independently ($e^{-2k^i_+ s}$ or $e^{-2k^i_- s}$).

For distorted circularly polarized light, the following approximation is valid. When the analyzer is absent, Eq. (10) reduces to $I_\theta \propto I_\pm=(a_1\pm a_2)^2 e^{-2k^i_+ s}+(a_1\mp a_2)^2 e^{-2k^i_- s}$, where double signs refer to right and left elliptically polarized light, respectively. With no absorption $I_\pm=2(a_1^2+a_2^2)$. When the quality of circularly polarized light deteriorates, it is reduced, for example, to elliptically polarized light with 60% ellipticity, i.e., for $a_2=6a_1/10$,

$$I_+=(2a_1/5)^2[16e^{-2k^i_+ s}+e^{-2k^i_- s}]$$

and

$$I_-=(2a_1/5)^2[e^{-2k^i_+ s}+16e^{-2k^i_- s}].$$

Then the following approximation holds: $I_+\approx(2a_1/5)^2 e^{-2k^i_+ s}$ and $I_-\approx(2a_1/5)^2 e^{-2k^i_- s}$ because the spectral distributions of k^i_+ and k^i_- are mostly overlapped in the present case. Thus, even if the circularity of polarization is not perfect, the σ^+ and σ^- light in Fig. 4 can be approximately regarded as right and left circularly polarized light, respectively, with an uncertainty of around 7%.

In our experiment, the circularity of $\sigma^\pm$ light is 50–90 % for each beam before and after the absorption cell. The degree of ellipticity is measured to be almost the same for the light before and after the cell. Under these conditions, all measured spectra coincide within experimental errors of around ±5%. This coincidence may be due to the spectral shifts of great bulk and gross absorption profiles.

The large shift and broad width may conceal fine details due to optical pumping, which has a significant effect in a precise fluorescence measurement [16]. In our experiment, large effects are not observed for laser intensities of around 0.1 to a few μW/mm^2. Including the above uncertainty, however, the veracity of shift may be estimated to be better than 80–90 % for a modest evaluation.

The solenoid coil has a 70 cm length, a 6.5 cm inner diameter, and a 13.5 cm outer diameter and is cooled by circulating water. The coil produces a magnetic field of 0.015 T at 8 A. The cylindrically shaped Pyrex absorption cell placed in the center of the coil has a 7 cm length and a 5 cm diameter. The laser beam passes the center of the coil and the cell. Consequently, the uniformity of the magnetic field in the interaction region may be estimated to be better than 98%. The uncertainty of the electric current to the solenoid coil is less than 0.05 A. Therefore, the mean-field uncertainty may be estimated to be less than 0.0001 T.

The earth's magnetic field is not shielded because of its weakness (0.000 05 T) in comparison with the coil's field (0.015 T). The magnetic field of 0.015 T is adopted in this paper because this magnitude is neither too weak nor too strong for the Zeeman splittings of the Cs 6 $^2S_{1/2}$ and 6 $^2P_{3/2}$ fine-structure and hyperfine levels that constitute the D_2 line. For a weak magnetic field, the effect of Larmor precession is not clear (see Sec. V) and for a strong field the electric-dipole moment must be treated differently from Eq. (15). The effectiveness of the formalism described by Eq. (16) is limited to the intermediate strength of the magnetic field. For the Cs D_2 line, this is less than around 10 T. In addition, the coil used in this study produces a maximum magnetic field of 0.03 T.

The laser intensity is on the order of a few μW/mm^2. The absorption cell is at room temperature. The vapour pressure ($P_{\text{mm Hg}}$) of the Cs atom is given by the Nernst formula. The Cs atomic density is obtained as [12] $N_0=9.651\times10^{18}\ P_{\text{mm Hg}}/T$. For room temperature $N_0\approx10^9$–10^{10} cm^{-3}. For this optically thin vapor and the current laser intensity, the atoms may be presumed to interact with the laser beam independently. The cell is not coated and is not filled with a buffer gas in order to make the optical pumping and alignment effect as small as possible. Therefore, collisional effects may be mainly caused by the resonance broadening (γ_R), i.e., collisions between the same species. ($\gamma_R=1.965\times10^7 P_{\text{mm Hg}}/T$ MHz. For the present case, $\gamma_R=0.093$ MHz.)

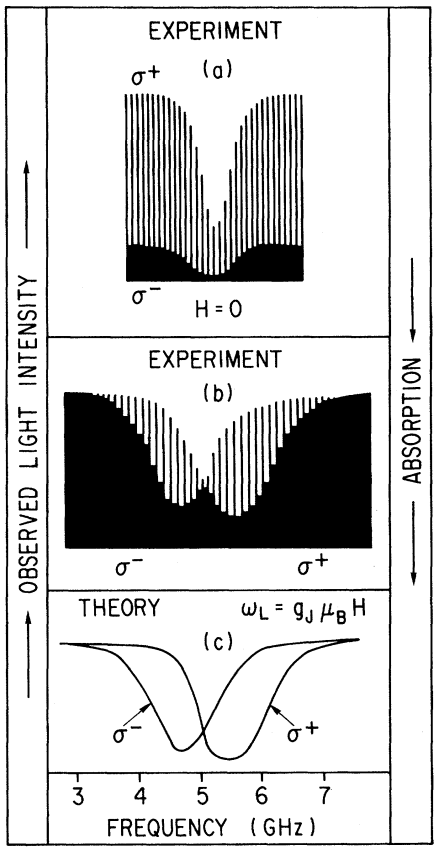

FIG. 5. (a) Measured absorption profiles in the absence of a magnetic field. (b) Typical experimental absorption profiles for $H=0.015$ T. (c) Theoretical spectra for $\omega_L=g_J\mu_B H$.

IV. RESULTS

The experimental results obtained by utilizing one of the methods of this theory are compared with the theoretical spectra of the Cs D_2, $F_g=3$ line for a magnetic field of 0.015 T (150 G). The level splittings that determine the spectral line distribution are derived from Ref. [17].

Figure 5(a) refers to the spectra in the absence of the magnetic field and the intensities of the incident σ^+ and σ^- light differ significantly. In Fig. 5(b) the typical absorption spectra for $\sigma^\pm$ light of equal intensity and a magnetic field of 0.015 T are shown.

The vertical lines are recorded as follows. When the chopper is open to σ^+ light, the amount of absorption of σ^+ light is recorded and when the chopper is open to σ^- light, its absorption is recorded. Thus the amount of absorption of $\sigma^\pm$ light is recorded reciprocally, sweeping the vertical lines.

The σ^+ and σ^- absorption profiles cross each other with distinct frequency shifts. The two envelopes refer to the absorption spectra of σ^+ and σ^- light, respectively. The abscissa refers to frequency. The laser intensity is adjusted by an attenuator.

Figure 5(c) shows theoretical profiles for $\sigma^\pm$ light that are obtained by assuming the Larmor frequency to be $\omega_L=g_J\mu_B H=420$ MHz, where $g_J=2.002$ is the ground-state fine-structure g factor of the Cs 6 $^2S_{1/2}$ state. The abscissa denotes the frequency measured from the Cs

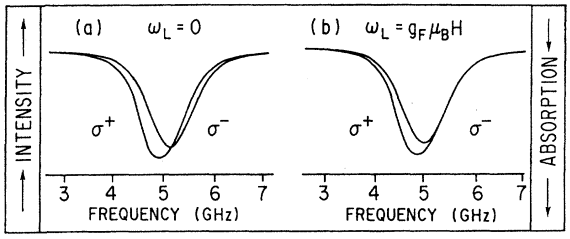

FIG. 6. (a) Profiles for $\omega_L=0$. (b) Profiles for $\omega_L=g_F\mu_B H$.

6 $^2S_{1/2}$–6 $^2P_{3/2}$ fine-structure transition frequency.

Figure 6(a) refers to $\omega_L=0$ (where the spectral line distributions correspond to those for $H=0.015$ T). Figure 6(b) shows profiles calculated with the assumption that $\omega_L=g_F\mu_B H=53$ MHz (g_F is the hyperfine g factor $=g_J/8$). These profiles do not reproduce the measured profiles. Therefore, from Figs. 5 and 6, it is concluded that the Larmor frequency is well defined by g_J, not g_F.

From experimental results [Fig. 5(b)] and theoretical profiles [Fig. 5(c)], the circular dichroism D can be estimated:

$$D=(I_\sigma^+-I_\sigma^-)/(I_\sigma^++I_\sigma^-), \tag{26}$$

where I_σ^+ and I_σ^- denote the σ^+ and σ^- components of detected intensity of the forward scattering light [18]. Figure 7 shows the circular dichroism D deduced from the above experiment and theory.

V. DISCUSSION

The Larmor frequency ω_L has been assumed to represent Zeeman splitting in a classical vector model. However, even for a weak magnetic field, the level splittings are not always linear: for example, the splittings are extraordinarily complicated for the Cs 6 $^2P_{3/2}$, $F_e=3$ state [17]. For the intermediate strength of the magnetic field also, the splittings of the 6 $^2P_{3/2}$ level are not simple. In this paper, it is taken into account that the Larmor precession does not induce the level splittings but provokes a phase shift of optical coherence through the Rabi frequency. The real resonance frequency is represented by ω_{21} in Eq. (21). The measured spectra [Fig. 5(b)] clearly show this effect of the phase shift.

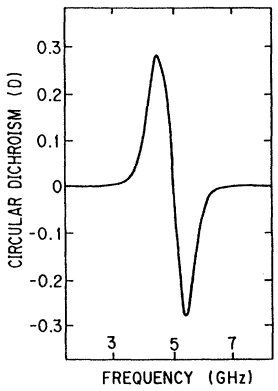

FIG. 7. Circular dichroism (D). Frequencies are measured from the Cs 6 $^2S_{1/2}$–6 $^2P_{3/2}$ fine-structure transition frequency.

Moreover, the magnitude of the shift is 420 MHz for $H=0.015$ T, which surpasses the Doppler width (226 MHz at $T=25$ °C). This shift, whose direction is opposite for σ^+ and σ^- components, cannot be attained by collisional interactions such as spin exchange, spin destruction, phase changing or phase destroying, and velocity changing collisions. These collisional effects (if any) are around several MHz and can be neglected compared to the magnitude of optical coherence shift.

When the magnetic field is absent, σ^+-, σ^--, and π-polarized light have the same transition probability and the same transition frequency. Therefore, the absorption profiles of σ^+ and σ^- light coincide, as shown in Fig. 5(a). As the laser intensity is on the order of several μW/mm^2, with a spectral width of about 20 MHz and the ground-state Zeeman splittings larger than 50 MHz for 0.015 T, it would be difficult to establish Zeeman coherence in the ground state.

In Fig. 5(b) the measured spectra of σ^+ and σ^- light are regarded as simple absorption spectra. Therefore, the circular dichroism is estimated in relation to parity nonconserving (PNC) rotation. The PNC rotation experiment [19–22] searches for optical rotation originating in admixtures of electric-dipole states (parity change) into the dominant magnetic-dipole transition (no parity change).

The circular dichroism D is related to refractive indices n^+, n^-, and n as [19]

$$(n^+-n^-)/(n-1)=2D. \tag{27}$$

Accordingly, the optical rotation Φ is given by

$$\Phi=(\pi L/\lambda)(n^+-n^-)=(2\pi L/\lambda)(n-1)D, \tag{28}$$

where L refers to the cell length, λ to the wavelength, and n to the refractive index induced by the magnetic-dipole amplitude [19–21]. As the PNC experiment exploits the refractive index n induced by the magnetic-dipole amplitude, our approach is different. However, if n is regarded as the average refractive index of the Cs vapor, Φ may be assumed to be the magnetic-field-induced optical rotation. For the Cs vapor (10^{-7} Torr at room temperature), $n-1\ll 1$.

VI. CONCLUSION

A general equation is constructed for the magneto-optical spectra. In this formalism, a laser beam of arbitrary polarization (linear, elliptical, or circular) is incident into an absorption cell placed in a static homogeneous magnetic field from an arbitrary direction to the field and detected through an analyzer with an arbitrary extinction ratio function (linear, elliptical, or any closed curve). The Faraday and Voigt formulas are deduced as special solutions of the general equation.

From the general equation, several facts are clarified. When the incident light is circularly polarized, the Faraday spectra give an absorption spectra of either right or left circularly polarized light and the birefringence term vanishes, whereas the generalized Voigt spectra contain absorption terms as well as interference terms. When the analyzer is absent, the generalized Faraday spectra for any polarized light give only absorption terms. Consequently, the effect of circular dochroism is evaluated without the influence of birefringence (Faraday rotation). From the generalized Faraday formula and the experiment utilizing it at 0.015 T, the existence of a virtual frequency shift due to Larmor precession that is twice as large as the Doppler broadening is verified for the Cs D_2 line.

[1] A. Corney, B. P. K. Kibble, and G. W. Series, Proc. R. Soc. London Ser. A **293**, 70 (1966).
[2] F. A. Blum, K. W. Nill, and A. J. Strauss, J. Chem. Phys. **58**, 4968 (1973).
[3] S. Giraud-Cotton, V. P. Kaftandjian, and L. Klein, Phys. Lett. **88A**, 453 (1982).
[4] K. H. Drake, W. Lange, and J. Mlynek, Opt. Commun. **66**, 315 (1988).
[5] F. Schuller, M. J. Macpherson, and D. N. Stacy, Physica **147C**, 321 (1987).
[6] L. M. Barkov, D. A. Melik-Pashayev, and M. S. Zolotorev, Opt. Commun. **70**, 467 (1989).
[7] I. O. G. Davies, P. E. G. Baird, and J. L. Nicol, J. Phys. B **20**, 5371 (1987).
[8] P. Junger, T. Fellman, B. Stahlberg, and M. Lindberg, Opt. Commun. **73**, 38 (1989).
[9] I. Hirano, J. Quant. Spectrosc. Radiat. Transfer **43**, 303 (1990).
[10] X. Chen, V. L. Telegdi, and A. Weis, J. Phys. B **20**, 5653 (1987).
[11] S. I. Kanorsky, A. Weis, J. Wulster, and T. W. Hänsch, Phys. Rev. A **47**, 1220 (1993).
[12] I. Hirano, Phys. Rev. A **50**, 4650 (1994).
[13] G. Karl, Can. J. Phys. **54**, 568 (1976).
[14] I. Hirano, J. Phys. B **26**, 3479 (1993).
[15] P. Tremblay, A. Michaud, M. Levesque, S. Thériault, M. Breton, J. Beaubien, and N. Cyr, Phys. Rev. A **42**, 2766 (1990).
[16] R. Walkup, A. L. Migdall, D. E. Pritchard, Phys. Rev. A **25**, 3114 (1982).
[17] I. Hirano, Metrologia **21**, 27 (1985).
[18] G. J. Roberts, P. E. G. Baird, M. W. S. M. Brimicombe, P. G. H. Sandars, D. R. Selby, and D. N. Stacy, J. Phys. B **13**, 1389 (1980).
[19] E. N. Fortson and L. Wilets, Adv. At. Mol. Phys. **16**, 319 (1980).
[20] J. D. Taylor, P. E. G. Baird, R. G. Hunt, M. J. D. Macpherson, G. Nowieki, P. G. H. Sandars, and D. N. Stacy, J. Phys. B **20**, 5423 (1987).
[21] P. E. G. Baird, M. W. S. M. Brimicombe, R. G. Hunt, G. J. Roberts, P. G. H. Sandars, and D. N. Stacy, Phys. Rev. Lett. **39**, 798 (1977).
[22] J. H. Hollister, G. R. Apperson, L. L. Lewis, T. P. Emmous, T. G. Vold, and E. N. Forston, Phys. Rev. Lett. **46**, 643 (1981).